Colloids and Surfaces A: Physicochemical andEngineering Aspects,
Volume 435, Special Issue SI, 20 Oct 2013,
doi: 10.1016/j.colsurfa.2013.02.051.

Colloids and suspended particulate matters influence on Ni availability in surface waters of impacted ultramafic systems in Brazil

I. Zelano[a,b], Y. Sivry,[a,*], C. Quantin[c], A. Gélabert[a], M. Tharaud[a], D. Jouvin[c], E. Montarges-Pelletier[d], J. Garnier[e], R. Pichon[c], S. Nowak[f], S. Miska[c], O. Abollino[b], O. and M.F. Benedetti[a]

[a] Univ. Paris Diderot, Sorbonne Paris Cité, Institut de Physique du Globe de Paris, UMR 7154, CNRS , F-75205 Paris, France

[b] Univeristà degli Studi di Torino, Via Pietro Giuria 5, 10125 Torino

[c] UMR 8148 IDES, Univ. Paris Sud-CNRS, 91405 Orsay Cedex, France

[d] CNRS, Université de Lorraine, Laboratoire Environnement et Minéralurgie, UMR 7569,, F-54500 Vandœuvre-lès-Nancy, France

[e] Universidade de Brasilia, IG/GMP-ICC Centro, 70919-970, Brasilia-DF, Brazil

[f] Univ. Paris Diderot, Sorbonne Paris Cité, ITODYS, UMR 7086, CNRS, F-75205 Paris, France

Highlights

- We tried to establish the link between nickel mobility and its suspended/colloidal bearing phases in natural waters from ultramafic systems.
- We performed Ni isotopic exchange kinetic on natural surface waters.
- We studied the properties and Ni speciation in suspended particulate matter (SPM) from a geochemical and mineralogical point of view.
- We demonstrated that metallurgical activity has a significant impact on Ni availability (both total amount and kinetics) in ultramafic systems.

Abstract

The overall objective of this work was to assess the modification of Ni availability and lability consequently to anthropic activity. Surface waters were collected in two ultramafic complexes (Barro Alto and Niquelândia) from Goías State (Brazil) impacted by mining and metallurgical activities. For the nearly first time, Isotopic Exchange Kinetic technique (IEK) was performed on these natural water samples to quantify the pool of isotopically exchangeable Ni from the suspended particulate matter (SPM) in water, defined here as E^{W}_{Ni}. The SPM mineralogy was investigated by X-Ray Diffraction (XRD), Scanning and Transmission Electron Microscopy (SEM and TEM). This allowed to establish the link between Ni availability and its solid speciation. Goethite, chlorite, talc and serpentine were identified as the main Ni bearing phases in SPM far from metallurgy (Barro Alto site) while in samples located in the area influenced by metallurgy (Niquelândia) Ni was mainly associated to spherical micrometric particles, related to fly ash produced by the ore combustion. In Niquelândia samples E^{W}_{Ni} value was found ranging between 2.4 and 565 µg L^{-1}, while in Barro Alto E^{W}_{Ni} was 62 µg L^{-1}, which corresponds to E_{Ni} values of 49000 and 2350 mg kg^{-1}, in SPM from Niquelândia and Barro Alto, respectively. Moreover, IEK experiments highlighted differences in kinetic of Ni exchanges: the maximum E^{W}_{Ni} value was reached after only 19 hours of interaction in Barro Alto sample, while in Niquelândia ones E^{W}_{Ni} hardly reached 70 to 95 % of the maximum after

the same period of time. On the one hand, both the low proportion and high velocity of Ni exchanges observed in Barro Alto sample may be attributed to surface complexation on talc, serpentine, chlorite and goethite. On the other hand, both the higher proportion of exchangeable stock and slower isotopic exchanges should be mostly attributed in Niquelândia samples to Ni interaction with the anthropogenic spherical and porous particles of Fe-Mg-Si-Al composition, related to FBA released by metallurgic activity.

Graphical abstract

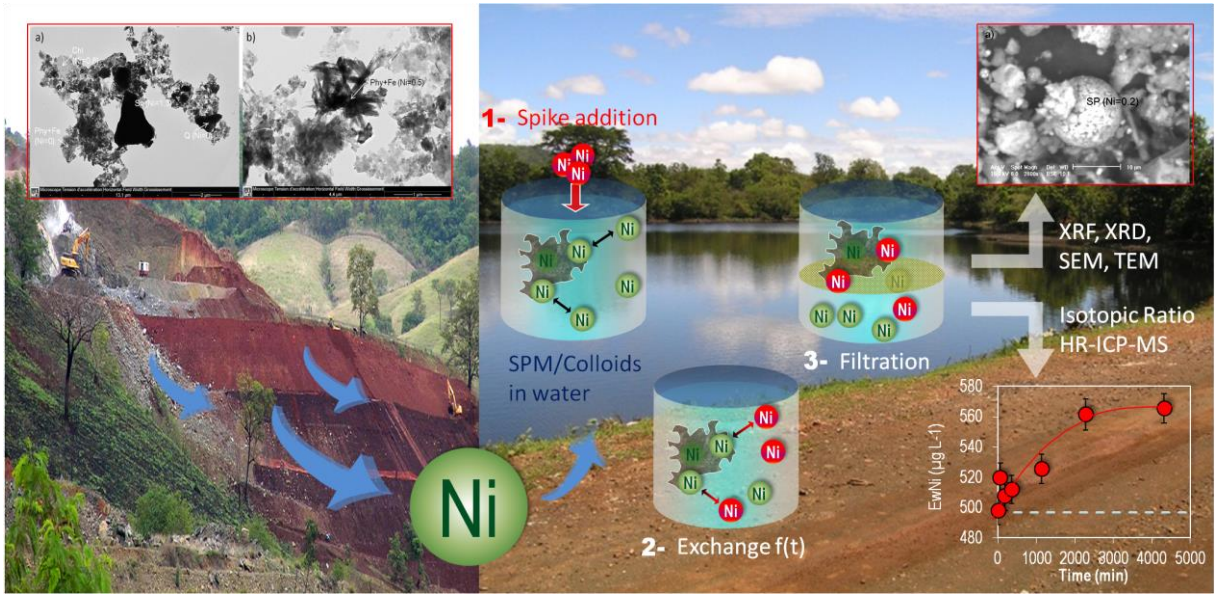

Keywords: Ni availability, Isotopic Exchange Kinetic, Surface water, Ultramafic system, goehtite, phyllosilicate, anthropogenic spherical particles, metallurgy.

1. Introduction

Mining and metallurgic industries are among the most invasive anthropic activities. They are known to generate important quantities of wastes, such as slags, ashes, spoils and liquid discharges [1-3]. In most cases, the generated wastes are stored on-site with no preliminary treatment [4, 5]. Since these by-products are usually associated to high metal concentrations, they are likely to contaminate the surrounding soils and surface waters through chemical weathering reactions [6]. As a result, the release and diffusion of potentially toxic elements associated to mining activities represent major environmental risks addressed in many studies, with important societal implications [7, 8].

Generally, in environmental settings exposed to contaminations, the resulting impacts and toxicity can hardly being inferred from the measure of the total metal concentration in the system. Instead, the chemical speciation is an essential parameter to be considered since the toxicity can vary significantly between the different chemical forms of a given element [9]. Consequently, metal bioavailability and toxicity are directly linked to its distribution between the different compartments of the aqueous medium (sediments, suspended particulate matter, water) [9]. Moreover, these compartments are not chemically dissociated, and the metal transfer dynamics among them constitute also a major control regarding their toxicity. Actually, metal mobility in environmental systems is governed by a complex array of complexation, adsorption, precipitation, redox reactions and physico-chemical parameters (pH, ionic strength, solid solution ratio...) which dictate metal ion solid-phase partitioning and speciation [10, 11]. For chemical elements, the most reactive fraction in a given system is frequently referred as “exchangeable pool” or “E value”. Several studies demonstrated that this exchangeable pool represented the main source of major elements and metals during plant uptake [12-14]. Then, the E value is usually considered a good approximation for the bioavailable pool in an environment, providing critical information regarding element biogeochemical cycling. In soils to assess the exchangeable metal pool, various techniques are commonly used, such as chemical extractions [15] and Diffusive Gradient in Thin Films (DGT) [16]. However, these approaches are not always adapted since they may require

preliminary chemical treatments (chemical extractions) or are hardly sensitive to short term kinetics (DGT). In this context, isotopic dilution (ID) and Isotopic exchange kinetics (IEK) techniques are conceptually attractive methods to discriminate between labile and non-labile metals since they do not affect the equilibrium of the system [17-19]. They also permit to access short term (minutes) as well as long term exchange kinetics, thus allowing to distinguish between different pools of available elements according to their rate of exchange kinetics. These differences in pool mobilization kinetics can be extrapolated to provide important information regarding the different exchange processes at stake, as well as an approximation of the binding modes between the exchangeable elements and their corresponding bearing phase [20]. As a result, ID is a powerful tool able to depict the potential evolution of solid-solution transfers in natural systems by focusing on the mobilization kinetics of an element in solution [21]. Many studies using ID for estimating element availability were already conducted on elements such as Al, As, Cd, Cr, Ca, Cu, Fe, F, K, Mg, Mn, N, Ni, Pb, S, Se and Zn [21, 22] and references therein.

Ultramafic soils (UM) are very unique ecosystems characterized by their floral, edafic and physiological peculiarities [23-26], their lack of mineral nutrients like P and K, and a strong chemical fertility limitation due to the low Ca/Mg ratio [27]. Moreover, they exhibit a high metal content such as Mn, Ni, Cr or Co, usually at harmful concentrations for the environmental systems [23, 28-31]. Due to the intense lateritic weathering of UM rocks, resulting in the formation of Ni lateritic ores, these areas are economically valuable for mining exploitation [32]. In the Goiás State (Brazil), three UM complexes (Barro Alto, Niquelândia and Cana Brava) occur and form one of the largest layered complexes in the world [33] with Ni reserves for the Barro Alto and Niquelândia complexes estimated to be higher than 100 million tons.

Subsequent to mining operations at these two locations, the mine wastes are deposited in storage basins generating aquatic colloids. These wastes exhibit Ni concentrations ranging between 1000 mg kg^{-1} and 3.2 % [34], and are directly in contact with both soils and vegetation. Therefore, along with the diffusion of the toxic elements through various

environmental compartments, a potential release of the contaminants in the surrounding areas can occur and needs to be addressed. Given their small size and high surface area, the suspended particles and colloids are known to be particularly efficient sorbents for metal ions, thus able to enhance Ni lability and to control its bioavailability [35]. However, to the best of our knowledge, the determination of the exchangeable pool to water-colloids systems using IEK technique is innovative and has little been reported before [36].

The overall objective of the present study is to evaluate the impact of mining activity on the Ni natural cycle. We specifically assess the Ni availability and we focus on its exchange kinetics from surface waters suspended material collected in altered and unaltered areas of two ultramafic complexes exploited for mining and metallurgy (Barro Alto and Niquelândia, respectively, in the State of Goias, Brazil). Sampling points were chosen in order to assess the potential impact of Ni mining and metallurgy on Ni availability in SPM and colloids. Isotopic Exchange Kinetics (IEK) were performed on samples of water interacting with ultramafic soils and ores on the one hand and with mine wastes on the other hand. The nature and mineralogy of suspended particulate matter and colloids were characterized to assess their control on Ni availability.

2. Material and Methods

2.1. Field settings

The study was carried out on the UM complexes of Niquelândia and Barro Alto inside an opencast mine and a metallurgical areas (Figure 1). The Niquelândia complex is about 40 km long and 20 km wide, whereas the Barro Alto complex is almost twice as long. The ultramafic bedrock related to Mesoproterozoic intrusion has been detailed [33, 37], and is mainly composed by dunite, peridotite, pyroxenite, more or less serpentinized [38]. These rocks are rich in mafic minerals (olivine, pyroxene, chromite) containing large amounts of metals like nickel. Soils developed from the UM bedrock at Niquelândia have been recently investigated [31] and were shown to consist mainly in Ferralsols and Cambisols (IUSS, 2006).

The climate is tropical, characterized by annual precipitation of approximately 1500 mm with a wet season from October to March. The mean temperature ranges between 18 and 22 °C. The vegetation consists of Cerrados, i.e. the Brazilian savannah, herbaceous plants and bushes on the ultramafic area, whereas a forest develops on the gabbros formations [25, 26]. The pyrometallurgical processing of the ore (a mixture of both lateritic and saprolitic materials) leads to the production of ferronickel. By-products are generated at different process stages; fine black ash (FBA), produced during the dehydration and calcination step, destined to be reprocessed because of its huge amounts of Ni (up to 23 g kg^{-1}) and slags produced during the smelting of the dehydrated material together with a reducing agent in an arc-furnace and the refining step.

2.2. Samples location, sampling and conditioning

Sampling points were chosen in order to assess the potential impact of Ni mining and metallurgy on Ni availability in SPM and colloids. For this purpose, four water systems were selected, corresponding to water directly in contact with mine by-products and runoff water in contact with UM soils and ores (Figure 1). The first one was taken in the Barro Alto site (BA), in a small stream collecting water runoff in the ore extraction area. Three samples were collected in the Niquelândia area: NIQ 1, NIQ 2 and NIQ 3. NIQ 1 was sampled in a storage basin for FBA. This basin also collects water runoff, which is therefore directly in contact with FBA. In addition, a sample of FBA that are stored in the vicinity of the banks was collected during the sampling campaign. NIQ 2 was collected in an artificial lake whose water is used for the cooling system of metallurgical plant. NIQ 3 sample was collected outside both the ultramafic and industrial sites areas in the lake "Serra de Mesa" (Figure 1). After collection, each bulk water sample was stored in pre-cleaned, acid-washed polyethylene bottles and divided in three subsamples: one was for IEK experiments, one was dedicated to the determination of total Ni content in bulk water (including dissolved, colloidal and particulate fractions) and one for the characterization of the colloidal fraction, here defined as filtered through 0.45 µm cellulose acetate membrane. An aliquot of the latter subsample was acidified with 15 N distilled nitric acid for further determination of major and trace elements

concentrations. Another aliquot was acidified with H_3PO_4 for dissolved organic carbon (DOC) concentration measurement and stored in specific glass vials and the remaining unacidified aliquot was used for determination of anions concentrations. All subsamples were stored at 4°C till analysis.

2.3. Characterization of suspended particulate matter

The SPM collected on filters was characterized using different techniques.

Total metal concentrations on filters were determined by X-ray fluorescence (XRF) using Panalytical X fluorescence spectrometer equipped with Energy Dispersive Minipal 4 (Rh X Ray tube-30kV-9W) at a resolution of 150 eV (Mn Kα). Measurements were performed according to the thin-layer hypothesis.

The mineralogical composition was determined using X-ray diffraction (XRD) analysis on a PANalytical diffractometer and using the Cu K_α radiation (at 45kV – 40 mA), in grazing incidence in the 5°-70° 2θ range with a scan step of 0.013°. XRD analyses were also performed after ethylene-glycol saturation to differentiate smectite from chlorite.

This mineralogical analysis was supplemented by microanalysis based on electronic microscopies. Backscattered electron images of the SPM were obtained using a Philips XL30 scanning electron microscope (SEM) operating at 15kV beam voltage, 1.5 µA beam current, equipped with an energy dispersive X-ray spectrometer (EDX-PGT Ge-detector ; acquisition time 40s). Particles and colloids on filters were also imaged with a Philips CM20 transmission electron microscopy (TEM) operating at 200 kV, at 50 000 and 110 000 fold magnification. Samples were prepared as follows: the filter was cut into small parts of a few square millimetres each, suspended in a few mL of ethanol and sonicated for 5 min. A drop of suspension obtained was then evaporated on a carbon-coated copper grid (200 mesh/100 µm) placed on filter paper. Elemental spectra were determined using EDS (EDX-PGT Ge-detector). The analyses were carried out in nanoprobe mode with a probe diameter of 10-20 nm. The kAB Kliff-Lorimer factors were determined using standards. Acquisition time was 40 s per measurement.

2.4. Chemical analyses

Conductivity and pH values were measured in the field using a WTW 3410 Set 2 multiparameter. The total nickel concentration in bulk water samples was determined on an aliquot of bulk water evaporated to dryness and acid-digested with a mixture of HNO_3–HF–HCl after removal of organic matter with H_2O_2 following the protocol from Sonke et al. [39]. Samples were then recovered with HNO_3. All reagents used were of analytical grade.

Trace and major elements concentrations were determined using a Thermo Fisher ICAP 6200 Duo ICP-OES. Detection limits were typically of 2 µg L^{-1} and the external precision was ± 5%. A Shimadzu TOC-VCSH analyser was used for measuring dissolved organic carbon (accuracy 1,5%, detection limit 100 µg L^{-1}). Anions concentrations were measured by Dionex Dx600 chromatography (accuracy ± 5% and detection limit Cl^- 7 µg L^{-1}, F^- 6 µg L^{-1}, NO_3^- 24 µg L^{-1}, SO_4^{--} 25 µg L^{-1}). Because it was not possible to measure it in the field, the alkalinity of samples were calculated as the difference between cations and anions concentrations.

2.5. Thermodynamic modelling

The results obtained by physical and chemical analyses were completed by thermodynamic calculations with the Visual MinteQ v. 3.0 code (Windows version of MinteQA2 v. 4.0 released by the USEPA) to evaluate if the solid phases detected were in thermodynamic equilibrium with the dissolved fraction. Concentrations of major elements measured in the water samples and the Visual MinteQ thermodynamic database were used for these calculations

2.6. Isotopic Exchange Kinetic Protocol

The spiking solution used for IEK experiments was enriched in stable ^{61}Ni (88.84% atom abundance) in a 0.4 M HNO_3 matrix and supplied by Spectrascan®. The experimental protocol was the same for all four samples: 125 mL of bulk water were spiked at *t=0* with 125 µL of ^{61}Ni spiking solution and put on an end-over-end shaker at 25±2°C. The kinetic experiment was performed the day after sampling and scheduled in order to obtain the amount of exchangeable metal immediately and after increasing durations (1min, 1h, 3h, 6h, 19h, 38h and 72h). For each time step, a 10 mL aliquot was filtered through a 0.45 µm

syringe filters. A 0.22 µm pore size is usually chosen in original IEK procedures [22]: nevertheless, preliminary tests revealed a strong clogging of these filters because these waters were very colloid-rich. The associated increase of filtration time prevent from any reliable kinetic study. Thus, in order to determine the impact of SPM size on the measured exchangeable pool, the last sampling point (after 72h) was successively filtered through 0.45 µm, 0.22 µm cellulose acetate and 1 kDa polyethersulfone membranes. To assess the reproducibility of the method, triplicates were performed for three sampling times (1min, 19h and 72h). Three filtration blanks were also performed to determine the filter and reagent contributions. Filtrates were acidified with 15N distilled HNO_3 and stored at 4°C. All filtrates, blanks and Ni spiking solution were weight-diluted in MilliQ water to reach a 1% HNO_3 matrix before High Resolution Inductively Coupled Plasma (HR-ICP-MS) analysis.

2.7. E value determination

The $^{61}Ni/^{58}Ni$ isotopic ratio was measured in the filtrate, the spike and the standard solutions using High-Resolution ICP-MS (ThermoScientific Element II). The measured Ni isotopes were ^{58}Ni-^{60}Ni-^{61}Ni-^{62}Ni and to correct possible isobaric interferences, ^{56}Fe-^{57}Fe were also measured. Each isotopic ratio corresponds to the average of 20 runs of 5 scans, allowing an internal analytical reproducibility better than 0.3% (2SD, n = 210). Within session, accuracy of the in-house isotopic reference material was checked every 8 samples and yielded less than 1% shift from the certified values. Most of the sub-procedural variation was found to be within the method's stated overall reproducibility (SE), determined on the three experimental replicates. The simultaneous analysis of the isotopic ratios of filtrate, spike and standard solutions prevented any need for correction of instrumental mass bias. The isotopically exchangeable amount of metal was then calculated as indicated by Sivry et al. [21] according to the formula adapted from Rodriguez-Gonzalez et al. [40]:

$$E_{Ni} = Q \times \frac{M_{STD}}{M_S} \times \frac{A_S}{A_{STD}} \times \left[\frac{(I.R.)_{Spike} - (I.R.)_{Sample}}{(I.R.)_{Sample} - (I.R.)_{STD}} \right] \quad (1)$$

Where Q represents the amount of added spike (µg per kg of suspended particulate matter), M_{STD} and M_S represent the atomic masses of Ni (in g mol^{-1}) in the standard and the spike

solutions, respectively, and A_{STD} and A_S represent the abundance percentage of ^{58}Ni, in standard and spike solutions, respectively. Natural isotope abundances were initially determined in bulk water samples and were consistent with those of the standard solutions used (*i.e.* typically within statistical uncertainty of the HR-ICP-MS analyses), hence the isotopic ratios within the standards were used to represent "natural abundances" in the E value calculations [21].

Because of the few amount of solid material collected on some filters, it was not possible to precisely quantify the exact weight of SPM and to express E_{Ni} per kg of SPM for all four samples. Hence, a new parameter E_{Ni}^{W} was introduced, which represents the amount of Ni exchanged per liter of solution (µg L^{-1}), defined as follows:

$$E_{Ni}^{W} = E_{Ni} * C_{SPM} \quad (2)$$

where C_{SPM} represents the mass concentration of SPM (kg L^{-1}). This parameter not only allows comparing results between all four water samples, but it also permits to establish a direct comparison between Ni exchangeable pool and dissolved Ni in a given natural water sample, which provides an interesting environmental approach. Both E_{Ni} and E_{Ni}^{W} results are expressed with corresponding uncertainties taking into account the standard deviations on each HR-ICP-MS analysis and on experimental replicates.

3. Results and discussion

3.1. Nickel bearing phases

The SPM elemental compositions were measured by XRF and the main element for each investigated site are reported in figure 2. Such technique performed on filters allows to detect the total amount of elements present in the irradiated surface area (0.5 cm^2). However, since the corresponding amount of SPM in the analysis volume is hardly quantifiable, the obtained results were normalized with Ti as a conservative element and are thus expressed as µg of element per µg of Ti. For BA, NIQ 1 and 3 samples, the major element is Si (with normalized ratio of 173, 4680 and 38, respectively) while NIQ 2 is somewhat different by exhibiting higher normalized ratio for Fe, Cl and Mg compared to Si (i.e. 182, 137, 97 and 72,

respectively). Actually the highest enrichments in Ni and Fe are found in NIQ 1 (184 and 1830, respectively) followed by NIQ 2 (23 and 182, respectively), BA (3 and 56, respectively) and NIQ 3 (<d.l. and 13, respectively). Such SPM compositions can be related to the main mineralogical components of the surrounding ores and soils. Rather counter intuitively, SPM after metallurgical process are more enriched in Fe and Ni than the one from the mining area. Therefore, one can assume that Fe/Ti and Ni/Ti enrichments in NIQ 1 and 2, are related to metallurgic activities since these samples were collected in metallurgy retention basins (i.e. into the metallurgical process influence zone). Similarly, Fe/Ti and Ni/Ti ratio in BA are mostly representative of the mining area (i.e. far from metallurgical process influence zone). Finally, given the small amount of Ni and Fe in NIQ 3 SPM, one can assume that the artificial lake "Serra de Mesa" is very slightly affected by the metallurgical ferronickel activity, despite a significant Cd enrichments in all NIQ samples.

Because of the small amounts of SPM, collected on filters for NIQ 2 and 3 samples, only BA and NIQ 1 samples displayed exploitable X-Ray diffractograms (figure 3). Qualitative analysis on BA sample diffractogram shows a SPM mineralogy dominated by chlorite (probably clinochlore), talc, serpentine, and goethite). The NIQ 1 X-Ray pattern displays a large contribution of amorphous material responsible for the low signal/noise ratio. Nevertheless, several crystalline phases can be identified like forsterite (Mg-olivine), serpentine, talc and magnetite or magnesioferrite (Figure 3). It is noticeable that all the identified clay minerals, as well as olivine, are potentially Ni bearing silicates commonly encountered in ultramafic soils [41-47], and goethite is known to be a great Ni scavenger in UM contexts [31, 48-53]. Moreover, Raous et al. [45] identified willemseite, a Ni-rich form of talc, in their garnieritic sample from Barro Alto. Interestingly, smectite was not detected in our samples, whereas it has been found in “garnieritic” and soil samples coming from Niquelândia massif [31, 42, 45, 46].

TEM observations reveal that SPM are heterogeneous both in terms of size distribution and mineralogical composition. Indeed, micrometric particles of quartz, aggregated particles of goethite and phyllosilicates (chlorite, serpentine but also kaolinite) can be identified in Barro

Alto SPM (Figure 4). These observations also suggest that goethite, chlorite and serpentine are the main Ni bearing phases in Barro Alto SPM, with Ni ranging from 0.5 to 1.3 at% (Figure 4), even though linking Ni content to phyllosilicate nature or amount of associated iron remains difficult given the multiplicity of potential bearing phases (Figure 4a-b). SEM and associated EDS study did not allowed to detect Ni in suspended matter from NIQ 3 filter. However, SEM investigations on NIQ 1-2 filters reveal the presence of phyllosilicates, chromite and spherical micrometric particles (2-10 µm), whose primary components are SiO_2 (8.5 - 20.5wt%), FeO (6 - 28wt%), MgO (2.1 - 10.2wt%) and Al_2O_3 (1.1 - 6wt%) associated in a glassy Fe-Mg-Al-Si matrix (Figure 5a-b-c-d). Some metallic inclusions and rims can be observed in the matrix and nickel concentration ranges from 0.5 to 2.5 at%. Similar spherical particles were observed by SEM investigations on Fine Black Ashe (FBA) picked up in the pond storage. Their surface appears heterogeneous and porous and they contain ferronickel inclusions with Ni concentrations comparable to NIQ 1 and 2 SPM (Figure 6). However, spherical particles observed on FBA sample are globally bigger in size (up to 60 µm). Thus, the smaller and lighter spherical particles of FBA deposited on the pond storage would readily be transported and suspended in water, while the biggest and heaviest ones settle in the basin. These spherical particles are typical of ash produced during metallurgic processes [54, 55]. They result from the combustion, melting and volatilization of ore minerals and commonly consist of slag and matte droplets, graphite, and condensed particles, which are collected by filters. When released to the atmosphere by smelting facilities, they are cooled in few seconds and remain essentially amorphous. These particles are quite similar to those studied by Lanteigne et al. [56] which were amorphous, porous, and which contained metals such as Ni. Furthermore, in NIQ 1, the presence of these spherical particles in significant quantities is likely to explain the presence of amorphous material in XRD diffractogram. Thus, given their high occurrence and their relatively elevated Ni content, these spherical particles of glassy nature are likely to constitute a major Ni bearing phase in NIQ 1 and 2 samples. Hence, Barro Alto site may be characterized by the association of Ni mainly with

goethite and clay minerals, while Ni in Niquelândia1 and 2 sites may be associated to micrometric spherical particles of anthropic origin.

3.2. Water chemistry

Concentrations of major elements, trace elements and DOC for the filtered water samples are reported in table 1, as well as conductivity, pH values and Ni total concentration of bulk solutions, i.e. unfiltered acid attack waters. The highest DOC concentration was measured for NIQ 1 and 2, with 65.9 and 3.2 mg L^{-1}, respectively, as well as the highest concentration of anions and major cations and the highest conductivity values (636 and 416 µS cm^{-1}, respectively).

The total Ni measured in sample BA is 443 µg L^{-1} while dissolved or colloidal (i.e. < 0.45 µm fraction) Ni is 42.5 µg L^{-1}. This indicates that only 10% Ni is dissolved or colloidal in this sample. This value is quite similar to that found for sample NIQ 3, with 7.4 µg L^{-1} for total Ni and 1.2 µg L^{-1} for < 0.45 µm Ni, which makes about 16% dissolved or colloidal Ni. These values are significantly different from the samples NIQ 1 (i.e. 898 µg L^{-1} for total Ni and 497 µg L^{-1} for < 0.45 µm Ni) and NIQ2 (i.e. 69.7 µg L^{-1} for total Ni and 47.3 µg L^{-1} for < 0.45 µm Ni) concentrations. Thus, about 56% and 68% of Ni is either dissolved or colloidal for NIQ 1 and NIQ 2 samples, respectively, whereas it is essentially carried by the SPM in NIQ 3 and BA samples. These Ni concentrations are extremely high compared to the global mean nickel concentration in rivers (0.65 µg L^{-1}) after Rauch and Pacyna [57], but closely related to results from Raous et al. [42]. These authors showed that limonitic and garnieritic spoil materials from Niquelândia massif could release up to 30 and 390 µg Ni L^{-1}, respectively, during laboratory percolation experiments.

The solid phases potentially at thermodynamic equilibrium in the systems were investigated using the Visual Minteq.v. 3.0 code, based on the four water compositions (Table 1). The saturation indexes for the potential solubility-controlling phases in the system were calculated and reported in table 2 (*i.e.* for saturation indexes higher than -0.5). Given the lack of information regarding the chemical composition of the organic moieties in our systems (e.g. partly resulting from high temperature processes during ore calcination for NIQ 1 and 2), the

DOC was considered as generic fulvic acids and modeled using the NICA-Donnan model [58]. Important differences between BA and NIQ samples can be observed regarding the system saturation with respect to Fe oxy-hydroxides. BA water is highly oversaturated in dissolved Fe. Given the usual fast precipitation kinetics of Fe oxy-hydroxides at circumneutral pH [59], very low free Fe concentrations should be found in system, and the observed oversaturation of Fe can be explained by the 0.45 µm cutoff membrane which allows the presence of both dissolved Fe and small colloidal Fe oxy-hydroxides [60] in the filtrate. Given results from Allard et al. [60] the smallest Fe oxy-hydroxides are likely to consist in amorphous material (such as ferrihydrite) whereas the crystallized ones, like goethite, would be found in the SPM fraction. Similarly, these calculations display that BA water is oversaturated with respect to Al oxyhydroxides phases, suggesting the presence of Al in colloidal form [61] in solution.

In contrast to the BA water, the NIQ ones are not oversaturated with respect to Fe oxides. Indeed, NIQ 1 system seems to be mainly controlled by silicate phases with the potential occurrence of 1:1 (serpentine given as chrysotile in table 2), 2:1 (sepiolite) clay minerals, cryptocrystalline silica (chalcedony), and to a lesser extent Al phases such as diaspore. NIQ 1 water is also oversaturated with respect to cristobalite, a high temperature polymorph of silica. In addition, it is noticeable that Si oversaturation may result from a partial dissolution of the silica spherical particles identified earlier by SEM. However, the solubility constant of this amorphous material is not known, and has not been considered during thermodynamic modeling. Similarly to NIQ 1, NIQ 2 displays a possible equilibrium with silicates phases, but presents also the highest contribution of carbonate phases. However, given the uncertainties attached to alkalinity calculations, the equilibrium involving carbonated minerals have to be considered with caution, particularly the presence of $NiCO_3$ phases in NIQ 1 and NIQ 2. Finally, NIQ 3 is oversaturated with respect to diaspore and quartz only.

For the four sampling locations, the phases found to be potentially in equilibrium with the solution are in good agreement with those identified by XRD and EDS analysis. Interestingly, most of these phases are known to be possible Ni scavengers [48, 50, 62-64].

3.3. Nickel exchangeable pool

The amount of exchangeable nickel in water (E^{w}_{Ni} value) was calculated for each sampling time, giving a kinetic profile up to 3 days as reported in table 3 and figure 7. Given the total amount of nickel measured in the bulk water samples, the highest relative exchangeable pools (E^{w}_{Ni}%) are found in NIQ 1 and 2, with 63% and 72% of the total Ni, respectively, whereas E^{w}_{Ni}% represents 32% of total Ni in NIQ 3 (Table 3). Surprisingly, only 17% of the 443 µg L^{-1} of Ni contained in BA sample is exchangeable. From a kinetic point of view, IEK experiments clearly display two different trends between Niquelândia and Barro Alto samples. For all NIQ 1, 2 and 3 samples, E^{W}_{Ni} increases from initial values similar to dissolved Ni concentrations, 498, 45 and 0.6 µg L^{-1} respectively, to reach 565, 50 and 2.4 µg L^{-1} after 3 days of interaction (Table 3). On the opposite, in BA sample, E^{W}_{Ni} measured after 1 min is already almost twice the dissolved Ni concentration (73 µg L^{-1}) and this value remains constant over the length of experiment. To compare the exchange kinetics for the 4 sites, E^{W}_{Ni} values were normalized to the total exchangeable pool determined at 3 days of interaction, assuming 3 days are sufficient to reach Ni exchange equilibrium [22]. After 19 hours (1140 min) E^{W}_{Ni} in BA has already reached 100% of the maximum value, while NIQ 1-2 are between 90% and 95% and NIQ 3 less than 70%.

From a quantitative point of view also, significant differences among samples may be noticed: in 3 days, E^{W}_{Ni} value in NIQ 1 increases of 67 µg L^{-1}, while this increase is one order of magnitude lower for BA, NIQ 2 and NIQ 3 (11, 5 and 2 µg L^{-1}, respectively). Moreover, figure 7 shows that the major part of exchangeable Ni is in the dissolved fraction for NIQ 1 and 2, and the relative "stock" of exchangeable metal (i.e. metal associated to SPM, potentially released into the dissolved fraction) is low (12% and 5.4%, respectively). On the contrary, in NIQ 3 and BA samples, the relative E^{W}_{Ni} "stock" corresponds to 50% and 31%, respectively. This difference may partly result from the separation protocol with solutions filtered through 0.45 µm pore size membranes. Thus, one can assume that some colloidal Ni

could pass through the filters and be included in the Ni dissolved fraction although being associated to solid particles.

The impact of SPM size and particularly the role of colloids on the exchangeable pool was assessed by filtering the last sampling point (at 72h exposure time) successively through 0.45 µm, 0.22 µm and 1 kDa cutoff membranes. The results reported in figure 8 for BA sample indicate that the E^{W}_{Ni} measured in the 0.22 µm filtrate represents 78% of the one measured in the 0.45 µm filtrate, and is not significantly different from the 1 kDa one (i.e. 48.6, 62.0 and 47.8 µg L^{-1}, resp., Figure 8). For NIQ 1 sample, E^{W}_{Ni} value measured in the 0.22 µm fraction represents 86% of the 0.45 µm filtrate exchangeable stock, and is not significantly different from the 1 kDa one (i.e. 487, 565 and 479 µg L^{-1}, resp.). For NIQ 2 sample, E^{W}_{Ni} measured in the 0.22 µm and 1 kDa filtrates are 93% and 85%, respectively, of the 0.45 µm filtrate E^{W}_{Ni} (47, 43 and 50 µg L^{-1}, resp.). For NIQ 3, no significant concentration differences were measured between the various filtrates. This procedure allows to highlight i) large differences between the 0.45 µm and 0.22 µm fractions particularly in BA and NIQ 1 samples, and ii) shows that no significant difference in E^{W}_{Ni} values are measured when filtrating at 0.22 µm and 1 kDa for the four samples for all the experiments.

As noticed earlier, these results may be mitigated by the presence, in the <0.45 µm fraction, of colloids containing non-exchangeable Ni (i.e. structural Ni). This structural Ni may reduce the $^{61}Ni/^{58}Ni$ ratio in the measured filtrate, resulting in an overestimation of the corresponding calculated exchangeable metal. Given the important differences in BA and NIQ 1 for 0.45 and 0.22 µm, such an overestimation may potentially arise from the presence of colloidal Ni although not having been directly observed in these systems. A similar particles size impact on E^{W}_{Ni} has been previously reported for soil suspensions with evidences for non-reactive metal being contained within suspended colloidal particles (SCP-metal [65]). For example, Ma et al. [66] found that isotopically non exchangeable Cu associated with colloids accounted for up to 40% of the total Cu in the soil extracts. Surprisingly, these results reveal that colloids in these soil suspension samples hold a more important fraction of non-reactive metal than the bulk SPM. On the contrary, in the present study, such calculation displays that

non-reactive Ni contained in SCP would only account for 3% and 9% of the total Ni in bulk BA and NIQ 1 samples. For the four sites investigated, comparing E^{W}_{Ni} calculated in the 0.22 µm and the 0.45 µm filtrates shows a bias induced by non-reactive colloidal Ni being higher for BA compared to NIQ 1, 2 and 3, with 22%, 14%, 7% and 0%, respectively.

To summarize, IEK experiments display significant differences between BA and NIQ samples, regarding both the kinetic trends (very fast in BA, slower in NIQ samples) and the exchangeable pool of Ni (only 17% of total Ni in BA sample and from 32% to 72% of total Ni in NIQ samples). Moreover, Ni associated to the colloidal fraction (< 0.45 µm) is an important element to consider since it is able to induce overestimations in labile Ni for BA, and in a lesser extent for NIQ 1, 2 and 3 sites.

3.4. Linking Ni availability to its solid phase speciation

Quantitatively, the E_{Ni} values measured in BA SPM is significantly lower than in NIQ 1 SPM, with 2350 and 49000 mg kg^{-1}, respectively, corresponding to 9.1% and 42.4% of total Ni in SPM respectively (Table 3). These values are both significantly higher than those reported by Massoura et al. 2006 [63] for Ferralsols from New Caledonia (from 18 to 190 mg kg^{-1}). However, this difference would be reasonably explained by the difference in particle size (i.e. soils particles < 2 mm for Massoura et al.), and thus specific surface and overall reactivity, between the two studies.

The differences highlighted by IEK, between Ni exchangeable pools of BA and NIQ samples, may be related to the nature of suspended particulate matter. Some phyllosilicates such as talc and serpentine were detected on both BA and NIQ sites. However, SPM mineralogy in BA is differentiated from NIQ 1 and 2 by the occurrence of goethite and chlorite, and the absence of anthropogenic spherical particles. Assuming that Ni isotopic exchanges are related to surface sorption on SPM and colloids, both the low proportion and high velocity of Ni exchanges observed in BA sample may be attributed to interactions with surfaces of talc, serpentine, chlorite and goethite, all reported to be Ni complexants through surface processes [48, 50, 62-64, 67, 68]. The sorption of Ni(II) onto chlorite was shown by Zazzi et al. [68] to be strongly dependent on pH conditions, indicating surface complexation

processes. In addition, the pH of BA sample (7.7) corresponds to the stability window (7-9) of chlorite dissolution but also to the maximum Ni sorption capacity onto the chlorite surface. Low Ni availability in serpentine and chlorite has been reported for a wide range of different soils by Echevarria et al. [20] and Massoura et al. [63], and attributed to the presence of Ni in the crystal lattice. However, in ultramafic soils, Ni availability was found by Massoura et al. [63] and Chardot et al. [69] to increase with the occurrence of amorphous Fe oxides, the main contributor to Ni availability in their study, in the absence of smectite. It is noticeable that other studies show that Ni associated to goethite is predominantly included in the crystal lattice, and thus less available with respect to serpentine and chlorite or even unavailable [12, 20, 63, 70].

For Ni in NIQ 1 and NIQ 2 samples (and to a lesser extend for NIQ 3 sample), both the higher proportion of exchangeable stock and slower isotopic exchanges should be attributed to Ni interaction with the anthropogenic spherical and porous particles of Fe-Mg-Si-Al composition, related to FBA released by metallurgic activity. This fraction can strongly influence the kinetics of the exchange: equilibration between Ni isotopes may be slowed down because of Ni diffusion time through the porous amorphous matrix. Indeed, microporous and mesoporous silica materials are extensively used in water treatment for heavy metal sorption, separation and recovery [71, 72].

These results reveal i) a change in Ni exchange kinetics, and ii) an increase in Ni availability, between surface waters localized far or close to the metallurgical process influence zone. Thus, this anthropic activity significantly modify the nickel bearing phases and consequently enhance its (bio)availability. By extension, this traduces the impact of Ni mining and metallurgy on Ni availability on SPM and colloids and on the global Ni natural cycle.

4. Conclusion

Nickel lability and availability in SPM of surface waters is strongly dependent on the metal bearing phases. Considerable differences between Barro Alto and Niquelândia samples were assessed by IEK experiments. The maximum amount of available Ni was found in

Niquelândia water (565 µg L^{-1} *vs* 62 µg L^{-1} in Barro Alto) which is rich in fly ashes derived from pyrometallurgical activity. Both the low proportion and high velocity of Ni exchanges observed in BA sample may be attributed to interactions, through surface processes, with surfaces of talc, serpentine, chlorite and goethite, all reported to be Ni complexants. On the other side, the amorphous and porous spherical particles found in Niquelândia samples and related to fly ashes strongly control Ni availability: the exchange kinetics are slower compared to Barro Alto and the Ni available pool increases. Therefore, performing IEK experiments on specific phases such as goethite, serpentine (lizardite) and chlorite, as well as on FBA would provide a complete understanding of the role and quantitative contribution of metal-bearing phases on Ni availability. The change observed both in Ni availability and exchange velocity, between surface waters localized far or close to the metallurgical process influence zone, reveals that anthropic activity like metallurgy significantly modify the nickel bearing phases, consequently enhance its (bio)availability and thus, affect the global Ni natural cycle.

Acknowledgements

This work was supported by the National French Program EC2CO from INSU-CNRS. The authors wish to thank Anglo American for access to field facilities. The two reviewers are gratefully acknowledged for their constructive and detailed comments.

References

[1] L.R.P. De Andrade Lima, L.A. Bernardez, Characterization of the lead smelter slag in Santo Amaro, Bahia, Brazil., Journal of Hazardous Materials, 189 (2011) 692-699.
[2] Y. Sivry, M. Munoz, V. Sappin-Didier, J. Riotte, L. Denaix, P. de Parseval, C. Destrigneville, B. Dupre, Multimetallic contamination from Zn-ore smelter: solid speciation and potential mobility in riverine floodbank soils of the upper Lot River (SW France), European Journal of Mineralogy, 22 (2010) 679-691.
[3] K.A. Hudson-Edwar, H.E. Jamieson, B.G. Lottermoser, Mine Wastes: Past, Present, Future, in: Elements 2011, pp. 375.
[4] H.E. Jamieson, Geochemistry and Mineralogy of Solid Mine Waste: Essential Knowledge for Predicting Environmental Impact, Elements, 7 (2011) 381-386.
[5] M.L. Garcia-Lorenzo, C. Perez-Sirvent, M.J. Martinez-Sanchez, J. Molina-Ruiz, Trace elements contamination in an abandoned mining site in a semiarid zone, Journal of Geochemical Exploration, 113 (2012) 23-35.

[6] C. Navarro-Hervas, C. Perez-Sirvent, M.J. Martinez-Sanchez, M.L. Garcia-Lorenzo, J. Molina, Weathering processes in waste materials from a mining area in a semiarid zone, Applied Geochemistry, 27 (2012) 1991-2000.
[7] K.L. Plathe, F. von der Kammer, M. Hassellov, J.N. Moore, M. Murayama, T. Hofmann, M.F. Hochella, The role of nanominerals and mineral nanoparticles in the transport of toxic trace metals: Field-flow fractionation and analytical TEM analyses after nanoparticle isolation and density separation, Geochimica et Cosmochimica Acta, 102 (2013) 213-225.
[8] V. Ettler, P. Piantone, J. Touray, Mineralogical control on inorganic contaminant mobility in leachate from lead-zinc metallurgical slag: Experimental approach and long- term assessment., Mineralogical Magazine, 67 (2003) 1269-1283.
[9] H.E. Gabler, A. Bahr, B. Mieke, Determination of the interchangeable heavy-metal fraction in soils by isotope dilution mass spectrometry, Fresenius Journal of Analytical Chemistry, 365 (1999) 409-414.
[10] A.U. Rajapaksha, M. Vithanage, C. Oze, Nickel and manganeserelease in serpentine soil from the Ussangoda UltramaficComplex, SriLanka, Geoderma, 189-190 (2012) 1-9.
[11] R. Hamon, E. Lombi, P. Fortunati, A. Nolan, M.M. Laughlin, Coupling Speciation and Isotope Dilution Technique To Study Arsenic Mobilization in the Environment, Environmental Science & Technology, 38 (2004) 1794-1798.
[12] J. Garnier, C. Quentin, G. Echevarria, T. Becquer, Assessing chromate availability in tropical ultramafic soils using isotopic exchange kinetics, J Soils Sediments, 9 (2009) 468-475.
[13] E. Gérard, G. Echevarria, T. Sterckeman, J.L. Morel, Cadmium availability to three plant species varying in cadmium accumulation pattern, J Environ Qual, 29 (2000) 1117-1123.
[14] R.E. Hamon, J. Wunke, M. McLaughlin, R. Naidu, Availability of zinc and cadmium to different plant species., Aust J Soil Res, 35 (1997) 1267-1277.
[15] A. Tessier, P.G.C. Campbell, M. Bisson, Sequential Extraction Procedure for the Speciation of Particulate Trace Metals, Analytical Chemistry, 51 (1979).
[16] H. Zhang, W. Davison, B. Knight, S.P. McGrath, In situ measurements of solution concentrations and fluxes of trace metals in soils using DGT., Environmental Science and Technology 32 (1998) 704-710.
[17] Z.A. Ahnstrom, D.R.Parker, Cadmium reactivity in metal-contaminated soils using a coupled stable isotope dilution-sequential extraction procedure., Environmental Science & Technology, 35 (2001) 121-126.
[18] H.E. Gabler, A. Bahr, Enriched stable isotopes for determining the sorbed element fraction in soils in order to calculate sorption isotherm, Water-rock interaction, 1-2 (2001) 267-270.
[19] G. Echevarria, J.L. Morel, J.C. Fardeau, Assessment of phytoavailability of nickel in soils, Journal of Environmental Quality, 27 (1998) 1064-1070.
[20] G. Echevarria, S.T. Massoura, T. Sterckeman, T. Becquer, C. Schwartz, J.L. Morel, Assessment and control of the bioavailability of nickel in soils, Envieronmenta Toxicology and Chemistry, 25 (2006) 643-651.
[21] Y. Sivry, J. Riotte, V.r. Sappin-Didier, M. Munoz, P.-O. Redon, L. Denaix, B. Dupré, Multielementary (Cd, Cu, Pb, Zn, Ni) Stable Isotopic Exchange Kinetic (SIEK) Method To Characterize Polymetallic Contaminations, Environ. Sci. Technol., 45 (2011) 6247-6253.
[22] R.E. Hamon, D.R. Parker, E. Lombi, Advances in Isotopic Dilution Techniques in Trace Element Research: A Review of Methodologies, Benefits, and Limitations, in: Advances in Agronomy, Vol 99, Elsevier Academic Press Inc, San Diego, 2008, pp. 289-343.
[23] R.H. Whittaker, The ecology of serpentine soils.1.Introduction, Ecology, 35 (1954) 258-259.
[24] T. Jaffré, R.R. Brooks, J. Lee, R.D. Reeves, Sebertia acuminata: a hyperaccumulator of nickel from New Caledonia, Science, 193 (1976) 579-580.
[25] R.R. Brooks, R.D. Reeves, A.J.M. Baker, The serpentine vegetation of Goias state, Brazil. The vegetation of ultramafic (serpentine) soils. , Andover, 1992.
[26] R.D. Reeves, A.J.M. Baker, T. Becquer, G. Echevarria, Z.J.G. Miranda, The Flora and Biogeochemistry of the Ultramafic Soils of Goiás State, Brazil. , Plant Soil 293 (1997) 107-119.

[27] J. Proctor, Magnesium as a toxic element., Nature, 227 (1970) 742-743.
[28] R.H. Whittaker, The ecology of serpentine soils. 4. Th evegetation response to serpentine soils, Ecology, 35 (1954) 275-288.
[29] E. Bonifacio, E. Zanini, V. Boero, M. Franchini-Angela, Pedogenesis in a soil catena on serpentinite in north-western Italy, Geoderma, 75 (1997) 33-51.
[30] T. Becquer, C. Quantin, J.P. Boudot, Toxic levels of metals in Ferralsols under natural vegetation and crops in New Caledonia, European Journal of Soil Science, 61 (2010) 994-1004.
[31] J. Garnier, C. Quantin, E. Guimarães, V.K. Garg, E.S. Martins, T. Becquer, Understanding the genesis of ultramafic soils and catena dynamics in Niquelândia, Brazil, Geoderma, 151 (2009) 204-214.
[32] M. Elias, Nickel laterite deposits – geological overview, resources and exploitation., Giant Ore Deposits: Characteristics, genesis and exploration, (2001) 205-220.
[33] Ferreira-Filho, C. F., Kamo, S. L., Fuck, R. A., Krogh, T. E., Naldrett, A. J., Zircon and rutile U-Pb geochronology of the Niquelândia layered mafic and ultramafic intrusion, Brazil: constraints for the timing of magmatism and high grade metamorphism, Elsevier, Amsterdam, PAYS-BAS, 1994.
[34] C. Quantin, E. Montargès-Pelletier, D. Jouvin, L. C., A. Gelabert, Y. Sivry, R. Pichon, J. Garnier, Speciation and fractionation of nickel in pyrometallurgical by-products; consequences for ultramafic environments., in: Interface Against Pollution, Nancy, 2012.
[35] G.E. Brown, V.E. Henrich, W.H. Casey, D.L. Clark, C. Eggleston, A. Felmy, D.W. Goodman, M. Gratzel, G. Maciel, M.I. McCarthy, K.H. Nealson, D.A. Sverjensky, M.F. Toney, J.M. Zachara, Metal oxide surfaces and their interactions with aqueous solutions and microbial organisms., Chemical Reviews 99 (1999) 77-174.
[36] Y. Sivry, J. Riotte, B. Dupre, Study of exchangeable metal on colloidal humic acids and particulate matter by coupling ultrafiltration and isotopic tracers: Application to natural waters, Journal of Geochemical Exploration, 88 (2006) 144-147.
[37] G. Rivalenti, G. V.A.V., S. S., R. A., SienaF, The Niquelandia Mafic–ultramafic complex of Central Goias, Brazil.Petrological considerations, Rev. Bras. Geocienc., 12 (1982) 380-391.
[38] F.S. Oliveira, A.F.D.C. Varajao, C.A.C. Varajao, B. Boulange, N.S. Gomes, Bauxitisation of anorthosites from Central Brazil, Geoderma, 167-168 (2011) 319-327.
[39] J.E. Sonke, Y. Sivry, J. Viers, R. Freydier, L. Dejonghe, L. Andre, J.K. Aggarwal, F. Fontan, B. Dupre, Historical variations in the isotopic composition of atmospheric zinc deposition from a zinc smelter, Chemical Geology, 252 (2008) 145-157.
[40] P. Rodriguez-Gonzalez, J.M. Marchante-Gayon, J.I. GarciaAlonso, A. Sanz-Medel, Isotope dilution analysis for elemental speciation: a tutorial review, Spectrochimica Acta Part B, 60 (2005) 151-207.
[41] J.D. Grice, B. Gartrell, R.A. Gault, ERNIENICKELITE, NIMN3O7-CENTER-DOT-3H2O, a new mineral species from the Siberia complex, western Australia-Comments ont the crystallography of the chalcophanite group, Canadian Mineralogist, (1994) 333-337.
[42] S. Raous, T. Becquer, J. Garnier, É.d.S. Martins, G. Echevarria, T. Sterckeman, Mobility of metals in nickel mine spoil materials, Applied Geochemistry, 25 (2010) 1746-1755.
[43] A. Manceau, G. Calas, Heterogeneous distribution of nickel in hydrous silicates from New Caledonia ore deposits., Am. Mineral, 70 (1985) 549-558.
[44] M.A. Wells, E.R. Ramanaidou, Mineralogy and crystal chemistry of garnierites in the Goro lateritic nickel deposit, New Caledonia European Journal of Mineralogy, 21 (2009) 467-483.
[45] G.E.T.S. S. Raous, K. Hanna, F. Thomas, E.S. Martins, T. Becquer, Potentially toxic metals in ultramafic mining materials: Identification of the main bearing and reactive phases, Geoderma, 192 (2013) 111-119.
[46] G.W. Brindley, J.V. Desouza, Nickel-containig montmorillontes and chlorites from Brazil, with remarks on schuchardite, Mineralogical Magazine, 40 (1975) 141-152.
[47] G.W. Brindley, The structure and chemistry of hydrous nickel-containing silicate and nickel-aluminium hydroxy minerlas, Bulletin De Mineralogie, 103 (1980) 161-169.
[48] T. Becquer, C. Quantin, S. Rotte-Capet, Sources of trace metals in Ferralsols in New Caledonia, European Journal of Soil Science, 57 (2006) 200-213.

[49] G. J., Q. C., G. E., G. V.K., M. E.S., B. T., Understanding the genesis of ultramafic soils and catena dynamics in Niquelândia, Brazil, Geoderma, 151 (2009).
[50] R. Fan, A.R. Gerson, Nickel geochemistry of a Philippine laterite examined by bulk and microprobe synchrotron analyses, Geochimica et Cosmochimica Acta, 75 (2011) 6400-6415.
[51] Å. Zazzi, A.M. Jakobsson, S. Wold, Ni(II) sorption on natural chlorite, Applied Geochemistry, 27 (2012) 1198-1193.
[52] S.W. Bailey, Chlorites: structures and crystal chemistry., Madison,Wisconsin, USA, 1988.
[53] A.C.D. Newman, G. Brown, The chemical constitution of clay., in: A.C.D. Newman (Ed.) Chemistry of Clays and Clay Minerals., 1987.
[54] F. Juillot, G. Morin, P. Ildefonse, T.P. Trainor, M. Benedetti, L. Galoisy, G. Calas, G.E. Brown, Occurrence of Zn/Al hydrotalcite in smelter-impacted soils from northern France: Evidence from EXAFS spectroscopy and chemical extractions, American Mineralogist, 88 (2003) 509-526.
[55] A.G. El Samrani, B.S. Lartiges, J. Ghanbaja, J. Yvon, A. Kohler, Trace element carriers in combined sewer during dry and wet weather: an electron microscope investigation, Water Res, 38 (2004) 2063-2076.
[56] S. Lanteigne, M. Schindler, A.M. McDonald, K. Skeries, Y. Abdu, N.M. Mantha, M. Murayama, F.C. Hawthorne, M.F. Hochella, Mineralogy and Weathering of Smelter-Derived Spherical Particles in Soils: Implications for the Mobility of Ni and Cu in the Surficial Environment, Water Air Soil Pollut., 223 (2012) 3619-3641.
[57] J.N. Rauch, J.M. Pacyna, Earth's global Ag, Al, Cr, Cu, Fe, Ni, Pb, and Zn cycles, Global Biogeochemical Cycles, 23 (2009).
[58] D.G. Kinniburgh, C.J. Milne, M.F. Benedetti, J.P. Pinheiro, J. Filius, L.K. Koopal, W.H. VanRiemsdijk, Metal ion binding by humic acid: Application of the NICA-Donnan model, Environ. Sci. Technol., 30 (1996) 1687-1698.
[59] A.N. Pham, A.L. Rose, A.J. Feitz, Kinetics of Fe(III) precipitation in aqueous solutions at pH 6.0-9.5 and 25 degrees C, Geochimica et Cosmochimica Acta, 70 (2006) 640-650.
[60] T. Allard, N. Menguy, J. Salomon, Revealing forms of iron in river-borne material from major tropical rivers of the Amazon Basin (Brazil), Geochimica et Cosmochimica Acta, 68 (2004) 3079-3094.
[61] A. Dia, G. Gruau, G. Olivie-Lauquet, The distribution of rare earth elements in groundwaters: Assessing the role of source-rock composition, redox changes and colloidal particles, Geochimica et Cosmochimica Acta, 64 (2000) 4131-4151.
[62] S.K. Som, R. Jpshi, Chemical weathering of serpentinite and Ni enrichment in Fe oxide at Sukinda Area, Jajpur District, Orissa, India, Economic Geology and the Bulletin of the Society of Economic Geologists, 97 (2002) 165-172.
[63] S.T. Massoura, G. Echevarria, T. Becquer, J. Ghanbaja, E. Leclerc-Cessac, J.-L. Morel, Control of nickel availability by nickel bearing minerals in natural and anthropogenic soils, Geoderma, 136 (2006) 28-37.
[64] A. Manceau, M.L. Schlegel, M. Musso, S. V.A., G. C., P. P.E., T. F., Crystal chemistry of trace elements in natural and synthetic goethite, Geochimica et Cosmochimica Acta, 64 (2000) 3643-3661.
[65] E. Lombi, R.E. Hamon, S.P. McGrath, M.J. McLaughlin, Lability of Cd, Cu, and Zn in polluted soils treated with lime, beringite, and red mud and identification of a non-labile colloidal fraction of metals using isotopic techniques, Environ. Sci. Technol., 37 (2003) 979-984.
[66] Y.B. Ma, E. Lombi, I.W. Oliver, A.L. Nolan, M.J. McLaughlin, Long-term aging of copper added to soils, Environ. Sci. Technol., 40 (2006) 6310-6317.
[67] Å. Zazzi, A.-M. Jakobsson, S. Wold, Ni(II) sorption on natural chlorite, Applied Geochemistry, 27 (212) 1189-1193.
[68] A. Manceau, M.L. Schlegel, M. Musso, V.A. Sole, C. Gauthier, P.E. Petit, F. Trolard, Crystal chemistry of trace elements in natural and synthetic goethite, Geochimica et Cosmochimica Acta, 64 (2000) 3643-3661.
[69] V. Chardot, G. Echevarria, M. Gury, S. Massoura, J.L. Morel, Nickel bioavailability in an ultramafic toposequence in the Vosges Mountains (France), Plant and Soil, 293 (2007) 7-21.

[70] C. Quantin, T. Becquer, J.H. Rouiller, J. Berthelin, Oxide weathering and trace metal release by bacterial reduction in a New Caledonia Ferralsol, Biogeochemistry, 53 (2001) 323-340.
[71] L.X. Zhang, C.C. Yu, W.R. Zhao, Z.L. Hua, H.R. Chen, L. Li, J.L. Shi, Preparation of multi-amine-grafted mesoporous silicas and their application to heavy metal ions adsorption, Journal of Non-Crystalline Solids, 353 (2007) 4055-4061.
[72] M. Mureseanu, N. Cioatera, I. Trandafir, I. Georgescu, F. Fajula, A. Galarneau, Selective Cu2+ adsorption and recovery from contaminated water using mesoporous hybrid silica bio-adsorbents, Microporous and Mesoporous Materials, 146 (2011) 141-150.

Tables and Figures Captions

Table 1: Major and trace cations, anions and Dissolved Organic Carbon (DOC) concentrations (µg L^{-1}) of filtered water solutions, conductivity (µs cm^{-1}), pH values, sum of CO_2 species and total Ni concentration of bulk solution (µg L^{-1}).

Table 2: Saturation indexes for phases potentially in equilibrium with the water sample chemistry, as calculated using Visual Minteq v 3.1, are defined as S.I. = log (IAP/Ks). DOC taken as fulvic acids (NICA Donnan model).

Table 3: E^{W}_{Ni} values (µg of Ni per L of solution) calculated from 1 min to 3 days of interaction, and the corresponding proportion of the total Ni in bulk solution; E_{Ni} values for BA and NIQ 1 calculated after 3 days of interaction and expressed as mg of Ni per kg of SPM.

Figure 1: Map of the study area and location of plants, ores, tailings and sampling sites (red stars).

Figure 2. Total metal concentrations on SPM deposited on filters of BA, NIQ 1, 2 and 3 samples, normalized with Ti as conservative elements and expressed as µg of element per µg of Ti.

Figure 3: XRD patterns (Cu-Kα) of Barro Alto (BA) and Niquelândia (NIQ 1) suspended particulate matter. Mineral symbols are: F=forsterite, G=goethite, Sp= serpentine, M=magnetite or magnesioferrite, Chl=chlorite, T = talc.

Figure 4: Transmission electron micrographs of Barro Alto suspended particulate matter. Phy = undefined phyllosilicate, Fe = Fe oxide, Chl = chlorite, Sp = serpentine, Q = quartz. Ni concentration in atomic% determined by EDS.

Figure 5: Scanning electron micrographs showing the principal Ni-bearing phases in NIQ 1 (a and b) and NIQ 2 samples (c and d). SP : spherical particle composed mainly of Si-Fe-Mg-Al matrix, Phy = phyllosilicate. Ni concentration in atomic% determined by EDS.

Figure 6: Scanning electron micrograph (a) of a typical spherical particle (SP) sampled in a fine black ash deposit, in the vicinity of the deposit basin, and corresponding EDS spectra (b).

Figure 7: Exchangeable Ni in water (E^{w}_{Ni} values, µg L^{-1}) measured by stable IEK (red circles) and the corresponding dissolved Ni concentration (µg L^{-1}) (dashed lines, < 0.45 µm).

Figure 8: Isotopically exchangeable Ni (µg L^{-1}) measured in filtrates of BA, NIQ 2 and 3 samples (primary axis) and NIQ 1 sample (secondary axis) after successive filtrations through 0.45 µm (red circles), 0.22 µm (blue diamonds) and 1 KDa (white squares) cutoff membranes.

Table 1: Major and trace cations, anions and Dissolved Organic Carbon (DOC) concentrations (µg L^{-1}) of filtered water solutions, conductivity (µs cm^{-1}), pH values, sum of CO_2 species and total Ni concentration of bulk solution (µg L^{-1}).

	Dissolved metal concentrations												Bulk Conc.	Dissolved anion concentrations				DOC	Conductivity	pH	Σ CO_2 (calc.)
	(mg L^{-1})				(µg L^{-1})								(µg L^{-1})	(µg L^{-1})				(mg L^{-1})	(µS cm^{-1})		µM
	K	Mg	Ca	Na	Fe	Mn	Al	Si	Pb	Sb	Zn	Ni	Ni	F^-	Cl^-	NO_3^-	SO_4^{--}				
BA	0.176	11.246	1.620	0.370	44.4	9.6	18.7	10150	10.8	27.0	34.7	**42.5**	**443**	20	175	582	133	0.72	78.9	7.71	1083
NIQ 1	2.964	88.848	32.750	2.951	1449	452	34.5	30215	32.7	64.3	84.9	**497**	**898**	5049	7293	0	162080	65.9	636	8.02	5425
NIQ 2	2.632	55.272	23.540	2.726	4.4	1.9	0.0	18832	20.9	89.6	73.5	**47.3**	**69.7**	311	5450	677	70862	3.24	416	8.52	4260
NIQ 3	1.817	4.381	9.450	1.481	25.2	39.0	2.8	5011	4.6	31.1	30.7	**1.2**	**7.4**	52	765	135	981	1.82	75.2	7.35	922

Table 2: Saturation indexes for phases potentially in equilibrium with the water sample chemistry, as calculated using Visual Minteq v 3.1, are defined as S.I. = log (IAP/Ks). DOC taken as fulvic acids (NICA Donnan model).

		BA	NIQ 1	NIQ 2	NIQ 3
Al oxy-hydroxides	$Al(OH)_3$ (Soil)	0.805	-0.468	x	-0.246
	Boehmite	0.517	x	x	x
	Diaspore	2.222	0.949	x	1.171
	Gibbsite (C)	1.355	0.082	x	x
Fe oxy-hydroxides	Ferrihydrite	2.957	x	x	x
	Goethite	5.666	x	x	x
	Hematite	13.732	x	x	x
Silicated phases	Chalcedony	0.105	0.575	0.355	-0.2
	Chrysotile	x	1.849	3.947	x
	Cristobalite	-0.095	0.375	0.155	x
	Halloysite	1.724	0.12	x	x
	Kaolinite	3.864	2.26	x	x
	Quartz	x	1.025	0.805	0.25
	Sepiolite	x	1.981	3.013	x
Carbonated phases	Calcite	x	-0.232	0.762	x
	Dolomite (disordered)	x	-0.227	1.71	x
	Huntite	x	x	0.914	x
	Magnesite	x	x	0.348	x
	$NiCO_3$(s)	x	0.339	0.205	x

Table 3: E^{W}_{Ni} values (µg of Ni per L of solution) calculated from 1 min to 3 days of interaction, and the corresponding proportion of the total Ni in bulk solution; E_{Ni} values for BA and NIQ 1 calculated after 3 days of interaction and expressed as mg of Ni per kg of SPM.

	BA			NIQ 1			NIQ 2			NIQ 3		
Time (min)	**E^{w}_{Ni} (µg L^{-1})**	**SD**	**E^{w}_{Ni} (%)**	**E^{w}_{Ni} (µg L^{-1})**	**SD**	**E^{w}_{Ni} (%)**	**E^{w}_{Ni} (µg L^{-1})**	**SD**	**E^{w}_{Ni} (%)**	**E^{w}_{Ni} (µg L^{-1})**	**SD**	**E^{w}_{Ni} (%)**
1	72.7	7.4	16.4	498	9.2	55.4	45.2	1.5	64.9	0.6	0.1	8.1
60	74.2	7.5	16.8	520	9.6	57.9	45.4	1.4	65.2	<d.l.	<d.l.	<d.l.
180	74.7	7.6	16.9	507	9.3	56.5	45.1	1.4	64.7	<d.l.	<d.l.	<d.l.
360	72.3	7.4	16.3	511	9	57.0	44.3	1.4	63.6	0.8	0.3	10.4
1140	64.1	6.6	14.5	525	9.7	58.5	47.5	0.9	68.1	1.6	0.3	22.0
2280	59.3	6.0	13.4	561	10.3	62.5	48.9	1.5	70.1	1.2	0.2	15.7
4320	62.0	6.6	14.0	565	9.6	62.9	50.0	1.6	71.7	2.4	0.5	32.4
	E_{Ni} (mg kg^{-1})	**SD**	**E_{Ni} (wt%)**	**E_{Ni} (mg kg^{-1})**	**SD**	**E_{Ni} (wt%)**		--			--	
4320	2350	250	9.1	49000	830	42.4						

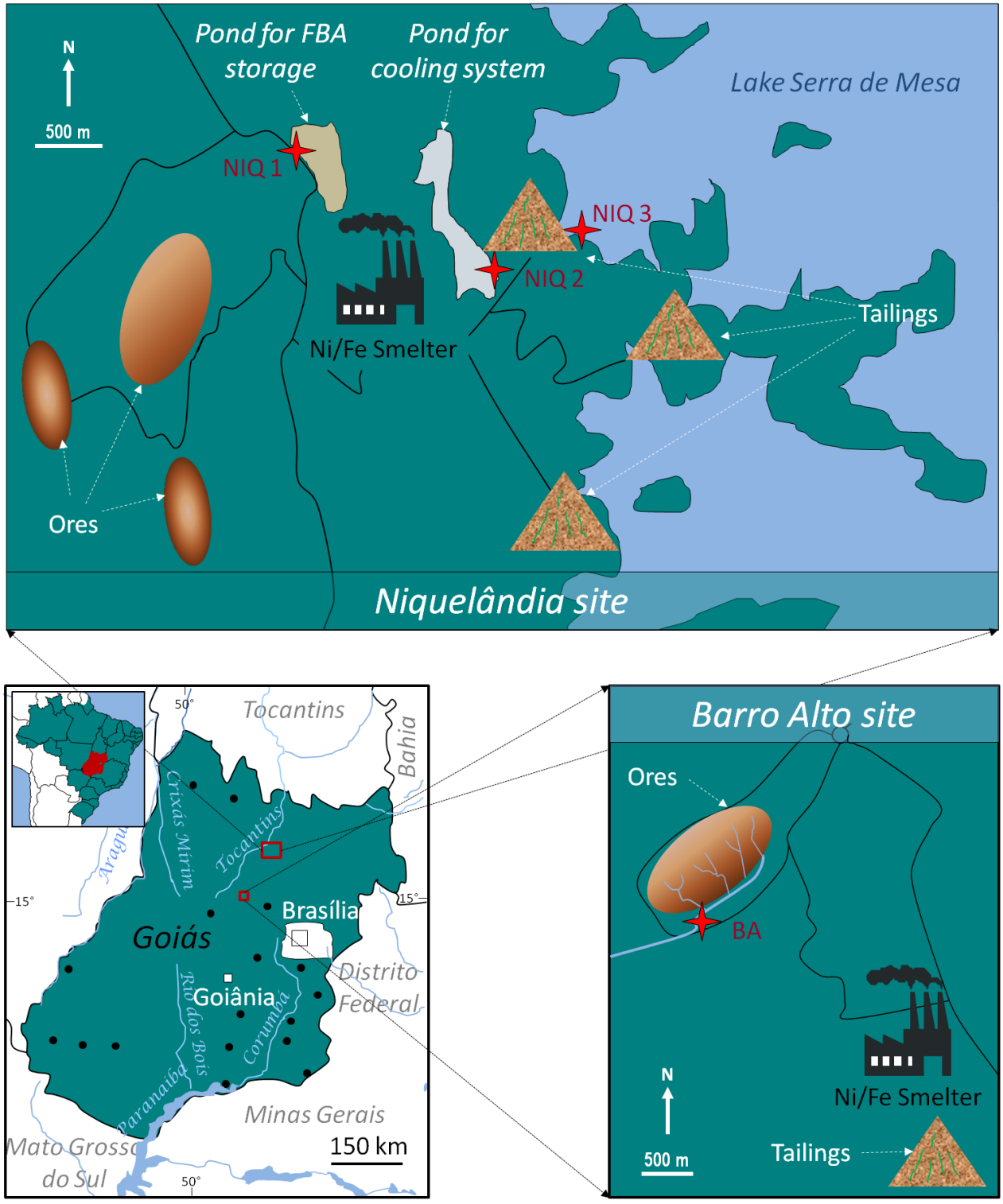

Figure 1: Map of the study area and location of plants, ores, tailings and sampling sites (red stars).

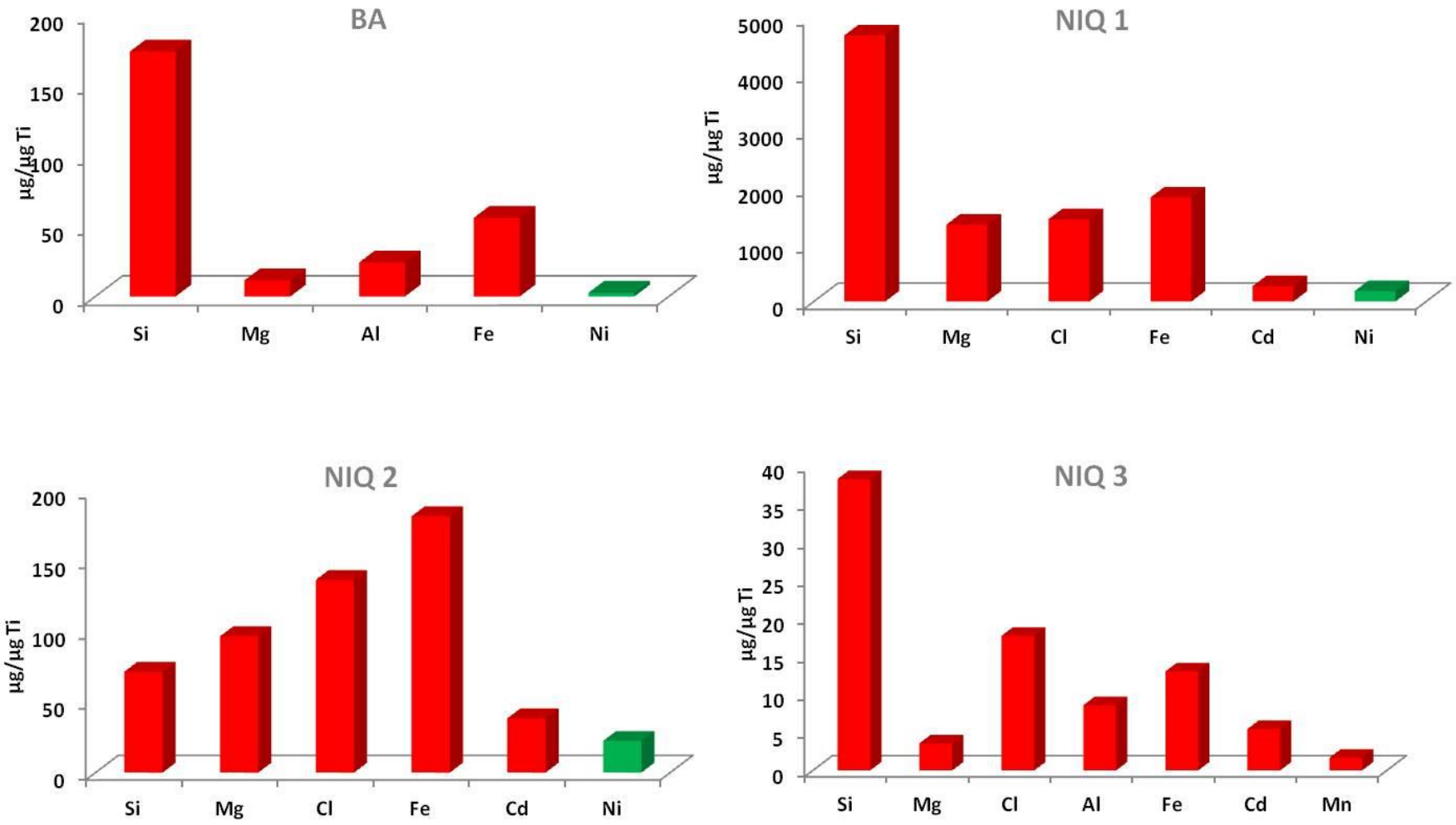

Figure 2. Total metal concentrations on SPM deposited on filters of BA, NIQ 1, 2 and 3 samples, normalized with Ti as conservative elements and expressed as µg of element per µg of Ti.

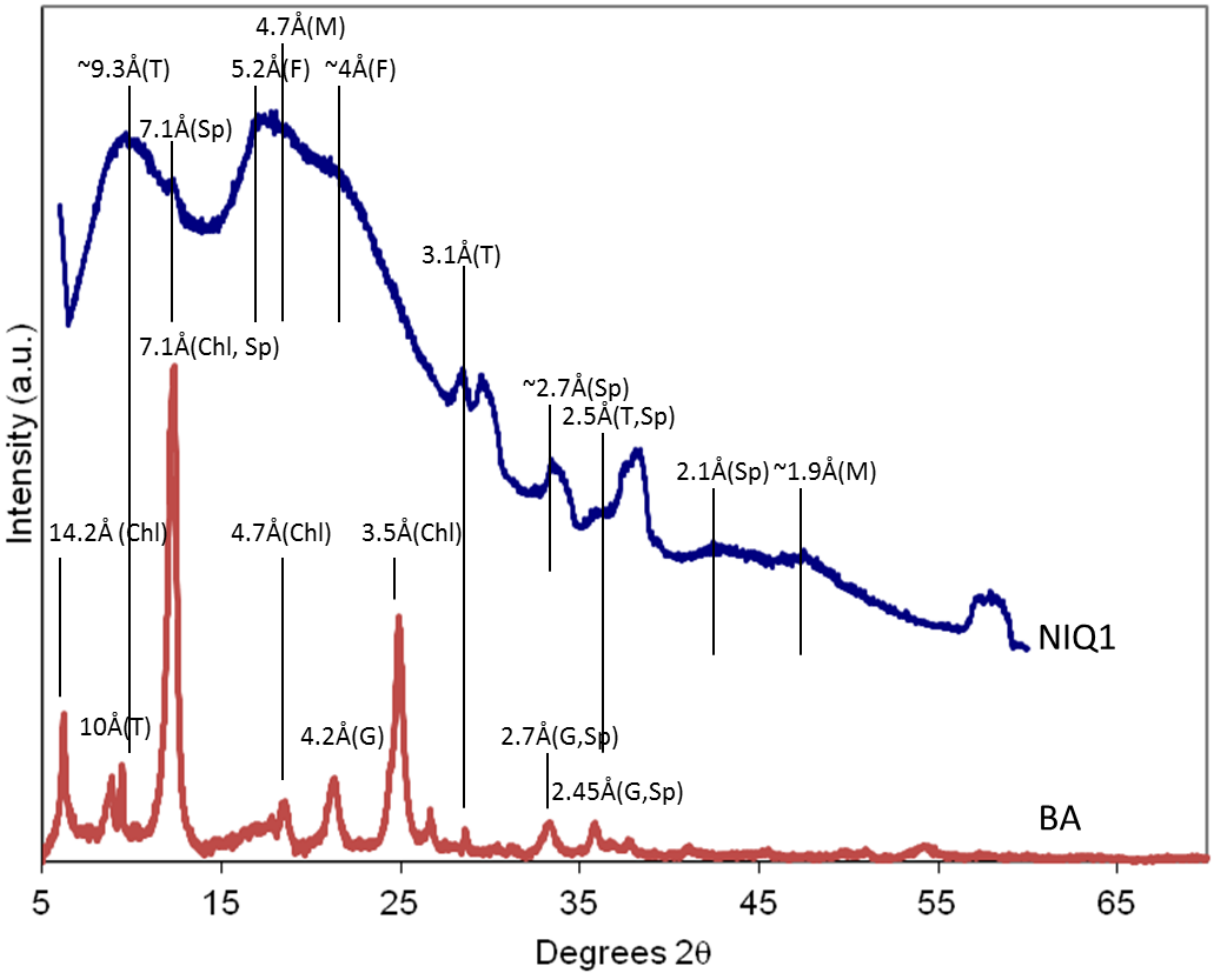

Figure 3: XRD patterns (Cu-Kα) of Barro Alto (BA) and Niquelândia (NIQ 1) suspended particulate matter. Mineral symbols are: F=forsterite, G=goethite, Sp= serpentine, M=magnetite or magnesioferrite, Chl=chlorite, T = talc.

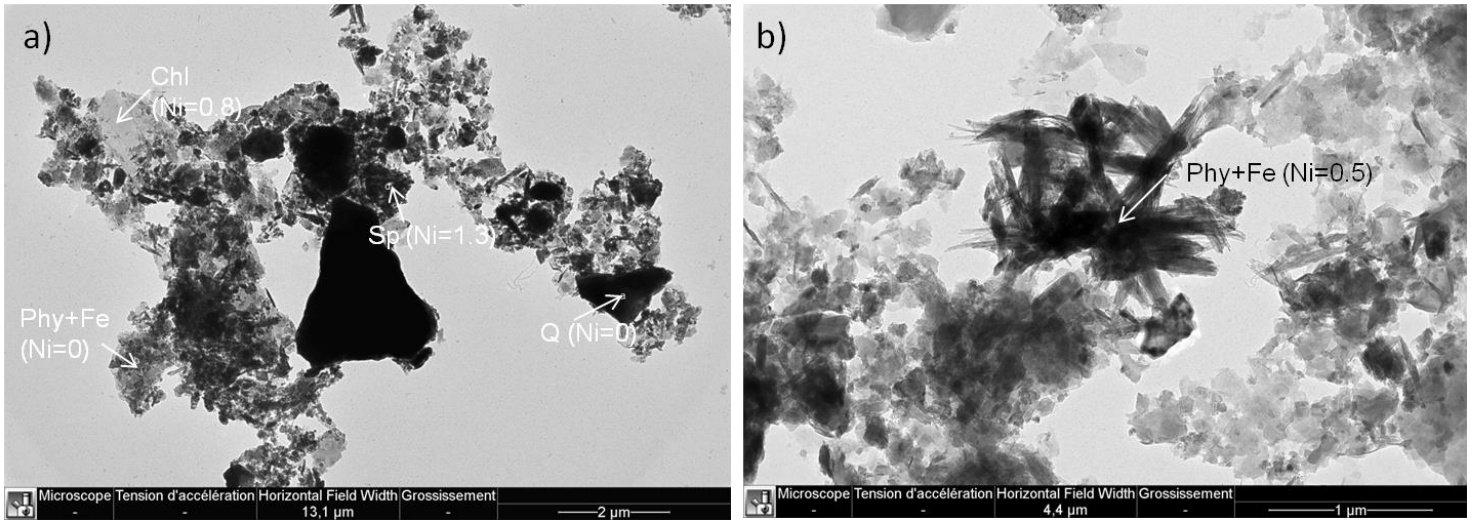

Figure 4: Transmission electron micrographs of Barro Alto suspended particulate matter. Phy = undefined phyllosilicate, Fe = Fe oxide, Chl = chlorite, Sp = serpentine, Q = quartz. Ni concentration in atomic% determined by EDS.

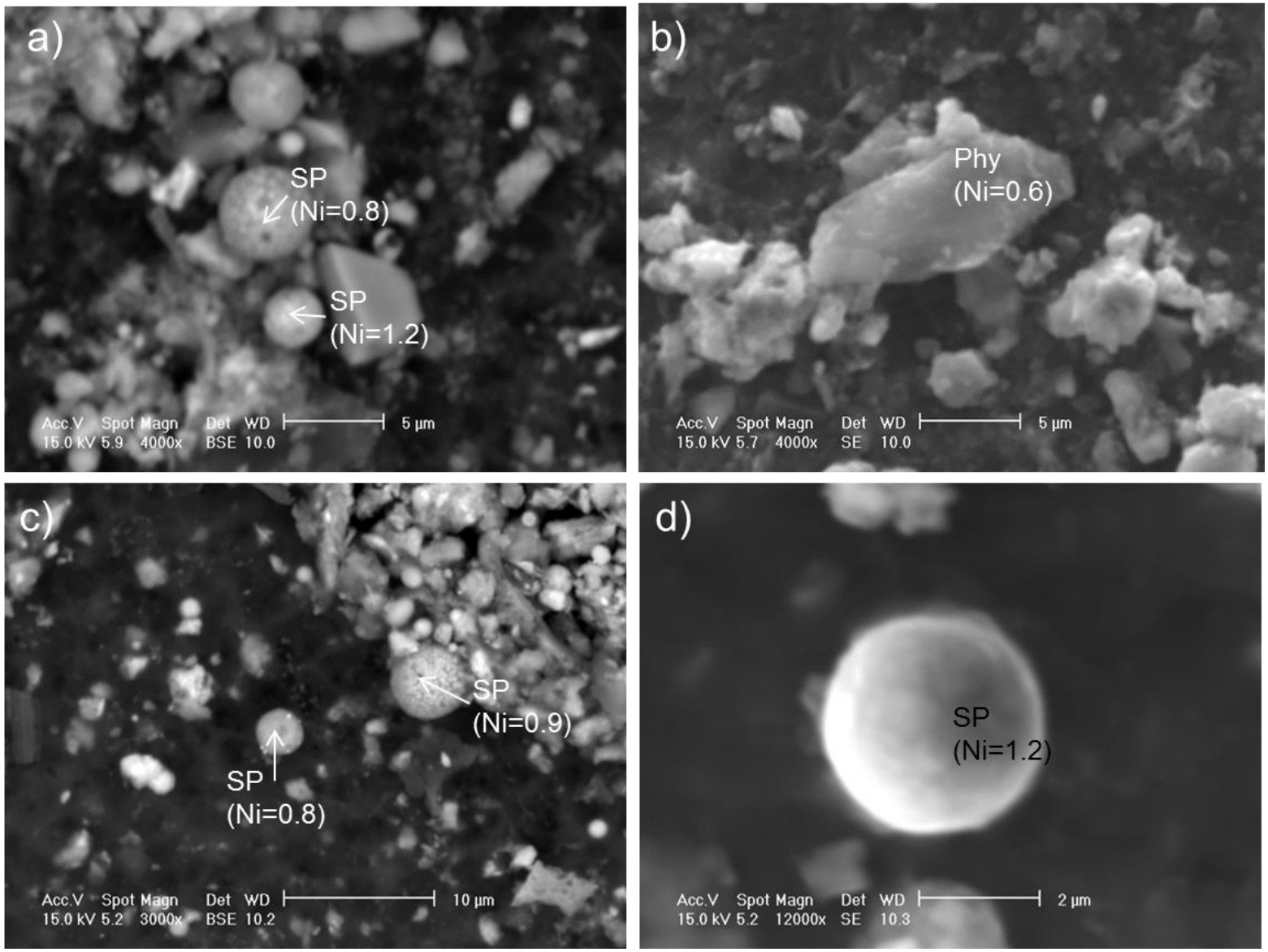

Figure 5: Scanning electron micrographs showing the principal Ni-bearing phases in NIQ 1 (a and b) and NIQ 2 samples (c and d). SP : spherical particle composed mainly of Si-Fe-Mg-Al matrix, Phy = phyllosilicate. Ni concentration in atomic% determined by EDS.

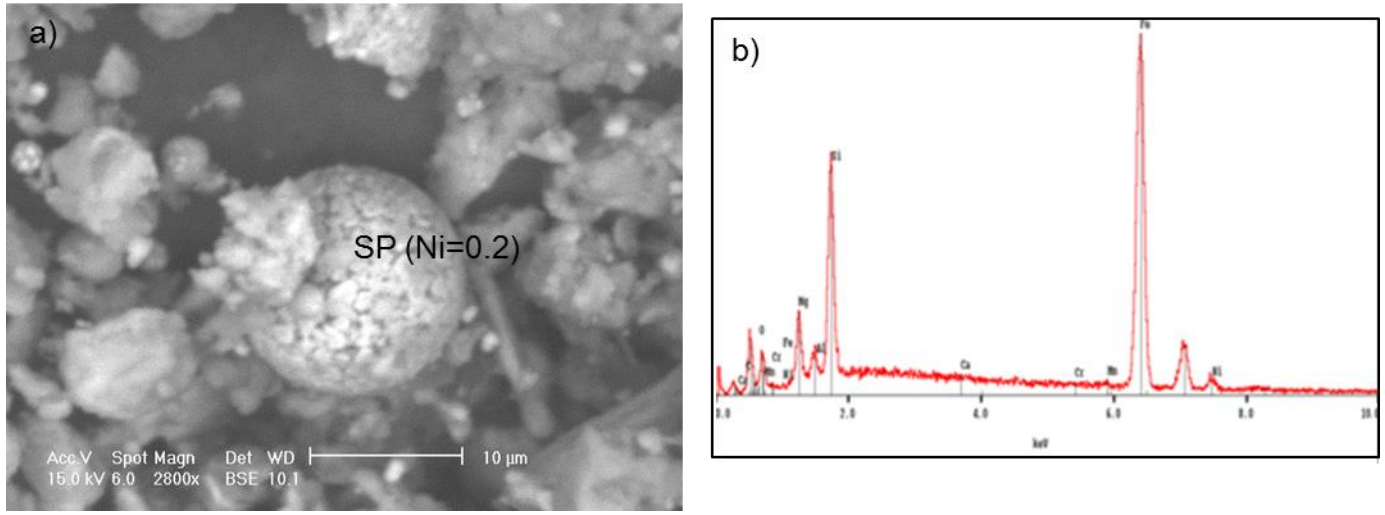

Figure 6: Scanning electron micrograph (a) of a typical spherical particle (SP) sampled in a fine black ash deposit, in the vicinity of the deposit basin, and corresponding EDS spectra (b).

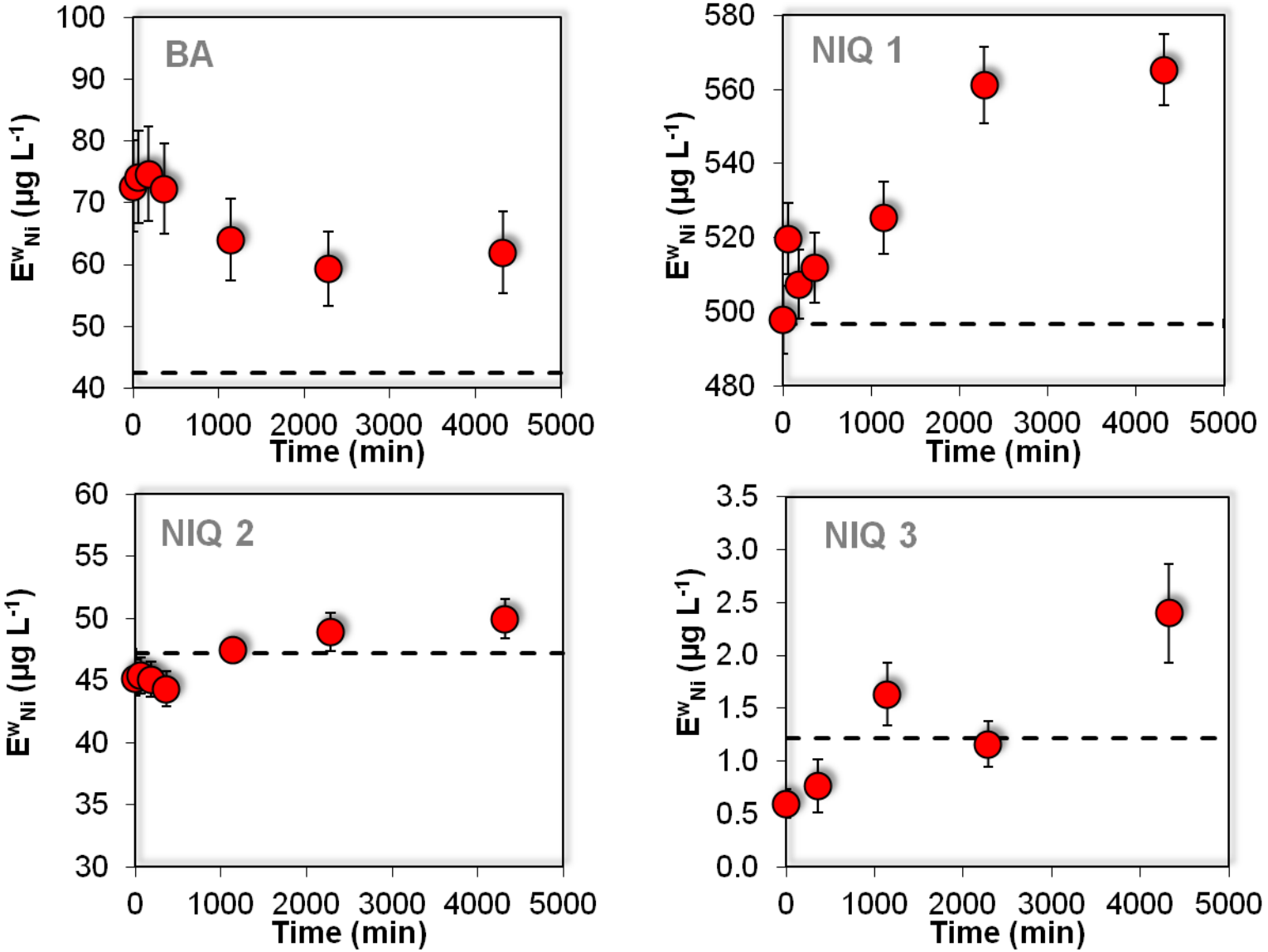

Figure 7: Exchangeable Ni in water (E^w_{Ni} values, µg L^{-1}) measured by stable IEK (red circles) and the corresponding dissolved Ni concentration (µg L^{-1}) (dashed lines, < 0.45 µm).

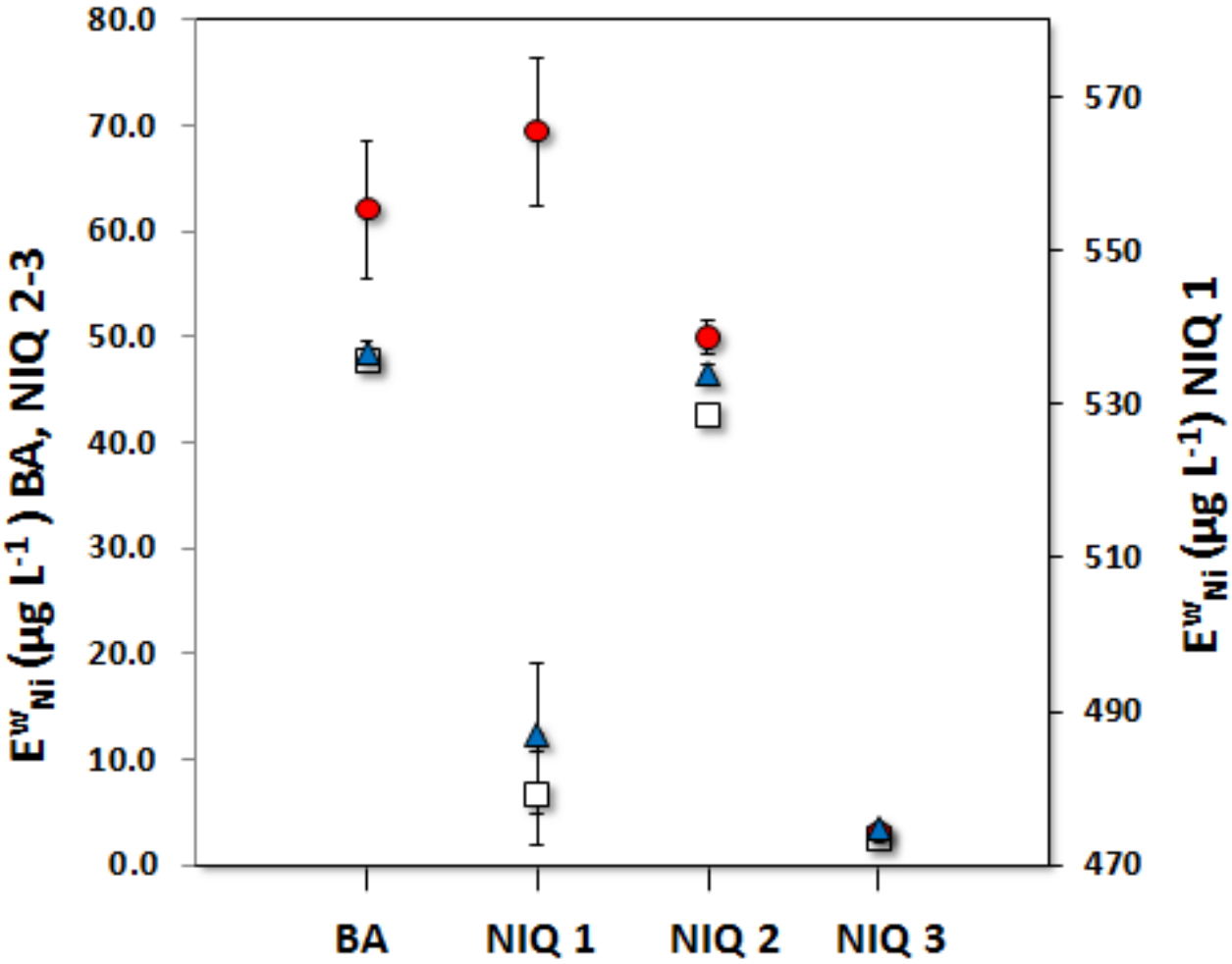

Figure 8: Isotopically exchangeable Ni (µg L^{-1}) measured in filtrates of BA, NIQ 2 and 3 samples (primary axis) and NIQ 1 sample (secondary axis) after successive filtrations through 0.45 µm (red circles), 0.22 µm (blue diamonds) and 1 KDa (white squares) cutoff membranes.